Magnetic confinement of electron and photon radiotherapy dose: A Monte Carlo simulation with a nonuniform longitudinal magnetic field

Yu Chen[a)]
Department of Physics, Randall Laboratory, University of Michigan, Ann Arbor, Michigan 48109-1120

Alex F. Bielajew
Department of Nuclear Engineering and Radiological Sciences, University of Michigan, Ann Arbor, Michigan 48109-2104

Dale W. Litzenberg and Jean M. Moran
Department of Radiation Oncology, University of Michigan, Ann Arbor, Michigan 48109-0010

Frederick D. Becchetti
Department of Physics, Randall Laboratory, University of Michigan, Ann Arbor, Michigan 48109-1120

(Received 14 December 2004; revised 6 July 2005; accepted for publication 7 July 2005; published 29 November 2005)

It recently has been shown experimentally that the focusing provided by a longitudinal nonuniform high magnetic field can significantly improve electron beam dose profiles. This could permit precise targeting of tumors near critical areas and minimize the radiation dose to surrounding healthy tissue. The experimental results together with Monte Carlo simulations suggest that the magnetic confinement of electron radiotherapy beams may provide an alternative to proton or heavy ion radiation therapy in some cases. In the present work, the external magnetic field capability of the Monte Carlo code PENELOPE was utilized by providing a subroutine that modeled the actual field produced by the solenoid magnet used in the experimental studies. The magnetic field in our simulation covered the region from the vacuum exit window to the phantom including surrounding air. In a longitudinal nonuniform magnetic field, it is observed that the electron dose can be focused in both the transverse and longitudinal directions. The measured dose profiles of the electron beam are generally reproduced in the Monte Carlo simulations to within a few percent in the region of interest provided that the geometry and the energy of the incident electron beam are accurately known. Comparisons for the photon beam dose profiles with and without the magnetic field are also made. The experimental results are qualitatively reproduced in the simulation. Our simulation shows that the excessive dose at the beam entrance is due to the magnetic field trapping and focusing scattered secondary electrons that were produced in the air by the incident photon beam. The simulations also show that the electron dose profile can be manipulated by the appropriate control of the beam energy together with the strength and displacement of the longitudinal magnetic field. [DOI: 10.1118/1.2011091]

Key words: electron therapy, dose confinement, magnetic fields, Monte Carlo

I. INTRODUCTION

The effect of magnetic fields on dose deposition has been studied for a long time. Bostick[1] proposed the use of longitudinal magnetic field for the enhancement of electron beam dose distributions. Shih's[2] Monte Carlo simulation followed by different experiments of Whitmire,[3,4] Nath,[5] and Paliwal *et al.*[6] reported the effect of transverse magnetic field enhancing electron-dose profiles in homogeneous and inhomogeneous media. Weinhous *et al.*[7] studied the enhancement of electron beam dose distributions by longitudinal magnetic fields of a single-coil superconducting magnet with Monte Carlo simulations. Bielajew[8] pointed out the erroneous Bragg peak effect for electron beams in uniform longitudinal magnetic fields and proved that for broad parallel beams, owing to lateral equilibrium, the central axis depth dose curve is independent of the strength of the external uniform longitudinal magnetic field. He demonstrated that a strong longitudinal magnetic field can significantly reduce the lateral spread of scattered and secondary electrons and hence the penumbra for electron and photon irradiations. In other words, a uniform longitudinal magnetic field shows its dose-enhancement effect only in places where the lateral charged particle equilibrium cannot be achieved originally. Monte Carlo simulations of Ramahi[9] and Naqvi *et al.*[10] further investigate the possibility and effectiveness of a longitudinal magnetic field to improve the photon dose profiles in regions around tissue-air interface such as upper respiratory cavities. Monte Carlo simulations for the application of a transverse magnetic field to control photon dose profiles also have been studied by Reiffel,[11] Li,[12] and David *et al.*[13] The experimental work by Litzenberg *et al.*[14] clearly demonstrated the application of a high magnetic field, a longitudinal nonuniform field in particular, can provide both transverse and longitudinal confinement of high-energy electron radiation therapy beams inside the phantom. This can then permit precise targeting of tumors near critical areas, enhance the dose in the

tumor region at greater depths, and the dose to surrounding healthy tissue can be suppressed. Relative to the enhanced dose at depths, the dose at the beam entrance region also can be reduced. This results in an internally focused, confined beam leading to a more localized, enhanced dose profile. Although electron linacs are the primary accelerator used to produce most clinical photon radiation therapy beams, the primary electron beam is seldom used for treating internal tumors. However, high-energy electron beams with a suitably focused and confined dose profile could prove useful as a cost-effective alternative to proton- and other ion-therapy beams, or as an additional modality in electron and photon radiation therapy.[15,16]

The main purpose of the present work was to accurately simulate the results of the existing experiment[14] and to understand the origin of a number of "anomalies" seen in the dose profiles obtained in the experiment. In this study the Monte Carlo code PENELOPE[17,18] was utilized to realistically simulate the experiment. The realistic magnetic field produced by the superconducting magnet was modeled in our simulations. It covered the whole region along the beam line from the vacuum exit window to the phantom including the surrounding air.

II. METHODS

The simulation algorithm of PENELOPE[17,18] is based on a scattering model that combines numerical databases with analytical cross-section models for the different interaction mechanisms and it is applicable to energies (kinetic energies in the case of electrons and positrons) from a few hundred eV to ~1 GeV. This code has been extensively tested without magnetic fields.[19,20] The arbitrary external magnetic field capability of PENELOPE was utilized by providing an efficient subroutine that looks up and interpolates the field map produced by a model of the nonuniform field of the solenoid magnet used in the experimental studies. The accuracy of the model will be described in Sec. II B.

A. Simulated setup

The high energy (G50) gantry of a two-gantry 50 MeV racetrack microtron accelerator (MM50 Scanditronix, Uppsala, Sweden) was used in the experiment.[14] We simulated the experiments for 20 MeV electron beams and 10 MV photon beams. Due to the high energy loss and scattering of electrons in materials, an accurate layout of all components in the beam path is required to do accurate simulations for electron beams. The gantry head was modeled with the following components: the beryllium vacuum exit window (0.0463 g/cm^2), the ion chamber made of gold and polyamide (0.0088 g/cm^2), the tungsten scattering foil (0.193 g/cm^2), the mylar gantry exit window (0.0024 g/cm^2), and helium gas (0.0116 g/cm^2).

The electron beam source before the vacuum exit window was modeled with a monoenergetic pencil beam. In the experiment, a helium bag was placed between the gantry and the magnet to reduce beam scattering.[14] An aluminum collimator of 5.08 cm thickness and 5.00 cm aperture was placed in the front side of the solenoid magnet bore. The phantom was placed directly behind the aluminum collimator in the solenoid magnet bore. The front surface of the phantom was about 17.16 cm from the center of the solenoid magnet. The experiment was designed so that the magnetic axis and the electron beam axis were coincident. The peak value of the magnetic field was 3.03 T at the center of the magnet.

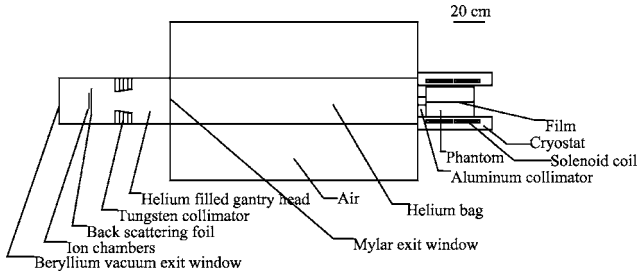

FIG. 1. Detailed setup used in the simulation. A pencil electron beam starts from the left vacuum exit window.

The overall setup used in the simulation is shown in Fig. 1. Figure 2 shows the detailed setup near the phantom where, again, accurate information is needed for simulations using electron beams, especially when nonuniform magnetic fields with strong gradients are present. The constituents of the plastic phantom (density 0.984 g/cm^3) are polyolefin (50%), polyurethane (46%), inert pigment (2%), and molecular sieves (2%).

The film used to obtain depth-dose measurements in the experiment was Kodak XV Ready Pack. As shown in Fig. 2, the phantom was a cylinder cut into two pieces along its axis with the film placed in between. The film was horizontal and the film plane was 0.5 cm lower than the magnet axis as the diameter of the phantom was somewhat smaller than the diameter of the magnet bore.

A superconducting solenoid magnet[21] (Intermagnetics General Corporation, Guilderland, NY) with 20-cm-diam bore was used to produce a longitudinal field with a maximum strength of about 3.03 T. The center of the magnetic field was approximately 249 cm away from the vacuum exit window[14] (Fig. 1).

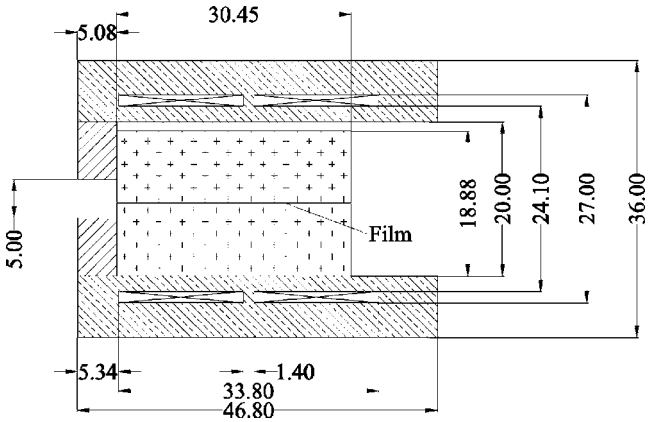

FIG. 2. The film is sandwiched horizontally between the two halves of the phantom (dimensions in cm).

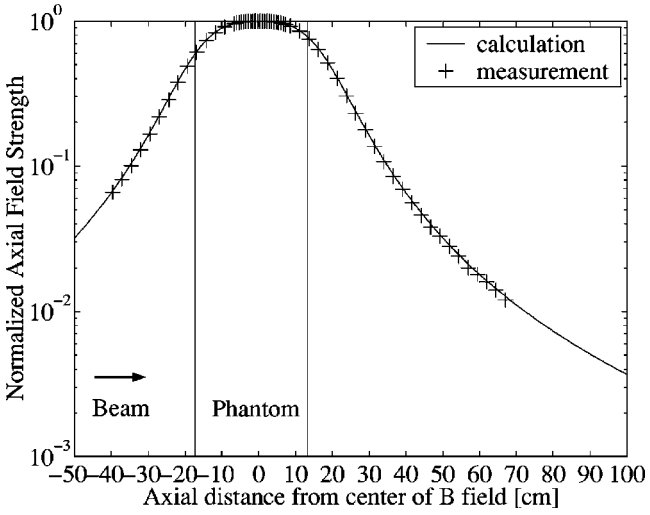

FIG. 3. The solenoid magnetic field along the central axis.

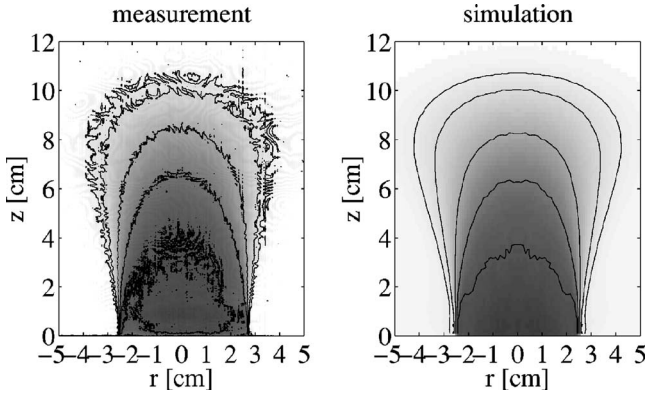

FIG. 5. Two-dimensional plot of 21.6 MeV electron dose profiles for $B=0$ T. Artifacts can be seen in the very low dose region (left). The 10%, 20%, 50%, 80%, and 100% isodose lines are shown. The dose is scaled to 100% at 3 cm on the central axis.

B. Magnetic field

The internal magnet configuration consists of solenoid coils of known dimensions.[22] The current density is approximated to be continuous in the finite cross-section area of the coil regions, hence the field can be numerically calculated with the Biot and Savart law. Since the magnet does not have a steel yoke, there is no hysteresis present, and the magnetic field scales directly in proportion to the current in the solenoid coil. The calibration curve is given in the manual of the magnet. The magnetic field strength at the center of the magnet was 3.03 T in the experiment. The calculated values along the axis are compared with the measured data in Fig. 3 and they agree to within 3% up to ±1 m from the center of the solenoid. Comparisons of off-axial longitudinal field strength measurements and calculations at several different axial positions were also made in Ref. 21. The calculated and measured values agree to within 2% inside the cryostat radius and within 5% out of the cryostat radius. The magnetic field strength and field lines are shown in Fig. 4. The calculated field profile is then stored in a look-up table. An interface subroutine was then written to make these data accessible to PENELOPE.

Different from the approximation used in this paper, the coils were approximated with an infinitely thin cylindrical current sheet to calculate the magnetic field in Ref. 14, which lead to differences near the coil regions compared with Fig. 4. The bore of the magnet is 20 cm in diameter and aperture of the collimator is 5 cm. Since the coils were blocked by the collimator and the shell of the magnet, the electrons could not reach this area. The closer to the axis, the smaller the difference is between these two models. These two approximations gave almost identical results near the axis if properly normalized. Dose calculations with the magnetic fields produced by these two approximations showed little difference.

Confinement using a longitudinal field is quite different than that using a transverse magnetic field which also has been suggested.[2–6,23] While a transverse beam can provide confinement, it also will deflect, rather than focus, the incident electron beam. In contrast, a longitudinal field generated by a solenoid magnet on the beam axis acts as a simple magnetic lens and provides both focusing (for the primary electrons) and confinement (for the secondary electrons) without deflecting the primary beam.

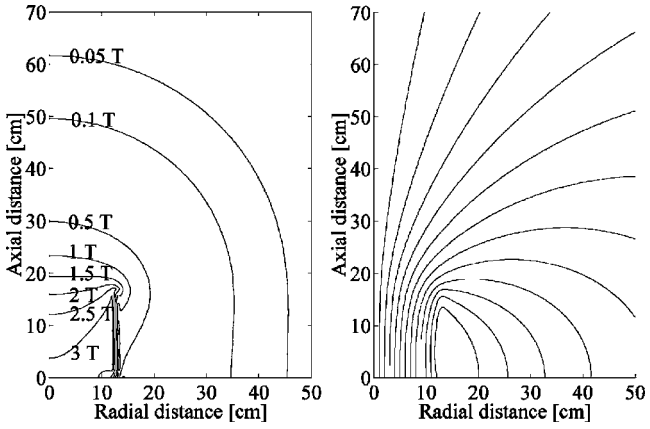

FIG. 4. The magnetic field strength distribution (left) and field lines (right).

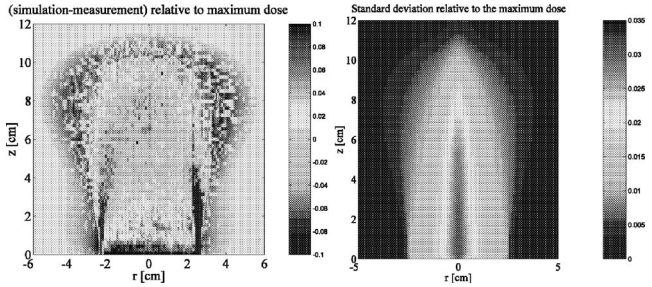

FIG. 6. The difference between the simulation and the measurement (left) together with the statistical uncertainty of the simulation for $E=21.6$ MeV and $B=0$ T (right).

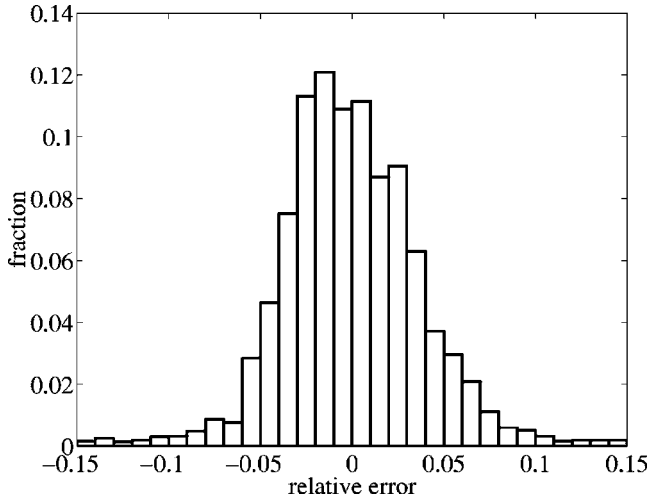

FIG. 7. The relative error (i.e., difference between MC simulation and experiment relative to the maximum dose) is tallied in the region where the dose lies in between the lower threshold 10% and the upper threshold 100% of the maximum dose. This histogram shows the fraction of the simulated data points with a certain relative error for $E=21.6$ MeV and $B=0$ T.

C. Normalization of the simulations to the measurements

The optical density of the film after irradiation was digitized and calibrated such that the optical density of the film is proportional to the dose.[14] Let $f(r,z)$ be the measured dose obtained from the film and $d(r,z)$ the calculated value from the Monte Carlo (MC) simulation. We expect

$$f(r,z) = kd(r,z), \tag{1}$$

where k is a normalization constant. Assume Eq. (1) is valid for any point of interest in the film.

Define the error as

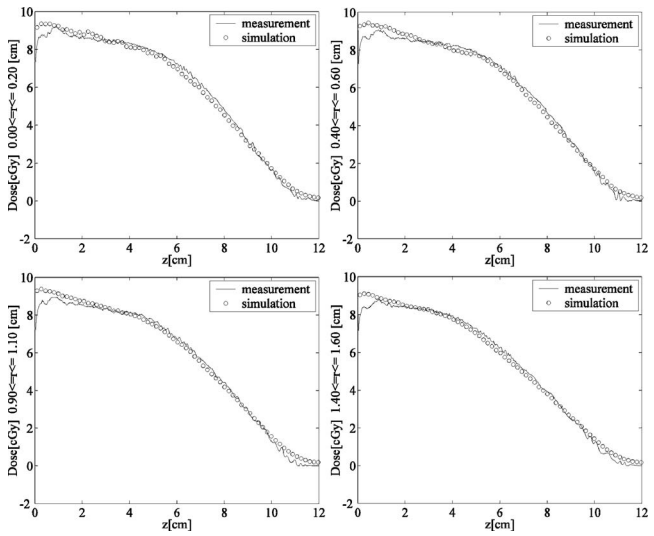

FIG. 8. The measured and simulated electron beam depth dose curves at central axis, 0.5, 1.0, and 1.5 cm away from the central axis for $E=21.6$ MeV and $B=0$ T.

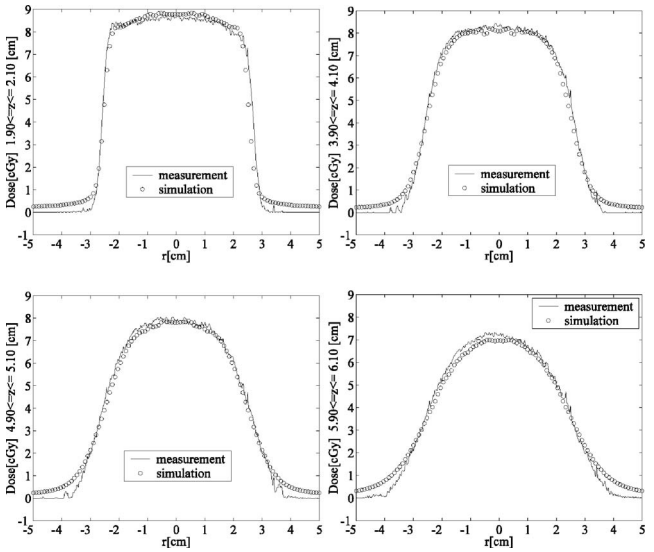

FIG. 9. The measured and simulated electron radial dose profiles at depth 2, 4, 5, and 6 cm for $E=21.6$ MeV and $B=0$ T.

$$\mathrm{Err} = \sum_{i,j} [f(r_i,z_j) - kd(r_i,z_j)]^2. \tag{2}$$

In the above expressions, $f(r_i,z_j)$ is the film data interpolated at the same position as for $d(r_i,z_j)$. Find k that minimizes Err, i.e., $d\mathrm{Err}/dk=0$. The summation is done over all the points that are within preset lower and upper limits. The lower limit was set to be 10% of the maximum dose while the upper limit was set to be 100% of the maximum dose. The reason to choose these numbers as the cutoffs is as follows. The XV film does not respond linearly over the whole range of interest, especially at high doses where it starts to saturate. Light leakage may affect the measurement of the very-low-dose region. Some artifacts can be seen in the dose plot for the case without magnetic field, which occurs where the dose is lower than that with the magnetic field. Since the highest dose in the experiment was still less than the saturation dose of the film, we set the upper limit to be 100%.

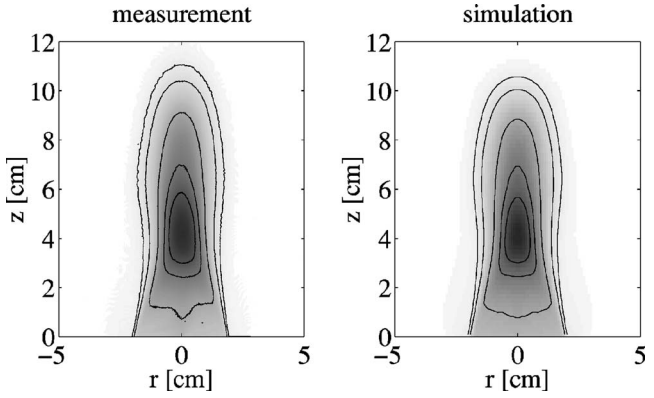

FIG. 10. Two-dimensional plot of 21.6 MeV electron dose profiles for $B=3.03$ T. The magnetic field is along z axis. The 10%, 20%, 50%, 80%, and 100% isodose lines are shown. The dose is scaled to 100% at 3 cm on the central axis.

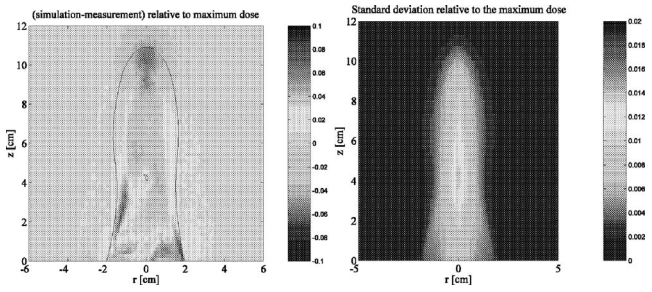

FIG. 11. The difference between the simulation and the measurement (left) and the statistical uncertainty of the simulation for $E=21.6$ MeV and $B=3.03$ T.

III. RESULTS

A. Electron beams

1. Electron beam dose distribution when magnetic field B=0 T

The stated energy of the electron beam could not exactly be verified in the experiment and was only known to about ±10% from the accelerator settings. Thus in the MC simulation, the first step was to determine the best-fit electron beam energy. This was done using the data taken without a magnetic field i.e., $B=0$ T. The actual beam energy was determined to be 21.6 MeV. This energy differs from the nominal energy 20 MeV used in the experiment as determined from the accelerator setting but this also has been found by other investigators.[24] Similar problems also were found in other medical accelerators.[25] This energy then was also used for the simulation when the magnetic field was applied.

The MC simulations are compared with measurements in Fig. 5 and the differences are shown in Fig. 6. One hundred million histories were simulated to make the statistical uncertainty smaller than 3% of the maximum dose everywhere (Fig. 6). We are primarily interested in the region where the dose ranges from 10% to 100% of the maximum dose and we can see from Fig. 7 that most of the simulation values agree with the measurement within a few percent in that region. The depth-dose curves at several radial positions are displayed in Fig. 8. The simulation agrees with the measurement reasonably well in the region 1 cm away from the phantom surface. The radial dose profiles at different depths are shown in Fig. 9. Without additional measurements of the dose in the first 1 cm, it is difficult to know the cause of the discrepancies between the model and the measurements in this region. Alignment of the sealed ready-pack film in the phantom is a potential source of error for the measurements.

2. Electron beam dose distribution when a longitudinal magnetic field is applied

The strength of the magnetic field at the center of the magnet was 3.03 T. Sixty million histories were simulated resulting in the statistical uncertainties smaller than 1.5% over the region of interest. The focusing effect in the dose profile of the electron beam is satisfactorily reproduced in the MC simulations (Figs. 10–14). As expected, in the longitudinal nonuniform magnetic field, it is observed that the electron dose can be focused in both the transverse and longitudinal directions. In addition, some electrons can be reflected backwards due to the "mirror" effect[26] of the magnetic field, enhancing the local dose (Fig. 15). The net result is that the high-dose region is now significantly confined in a much smaller volume when a strong longitudinal magnetic field is applied. The simulation agrees with the measurement quite well 1 cm from the surface into the phantom. Magnetic field data obtained with the thin sheet approximation were also tried to calculate the dose profiles. Similar results were obtained and the discrepancies in the region from the phantom surface until 1 cm deep could not be attributed to the small change of the magnetic field. Similar to the case with-

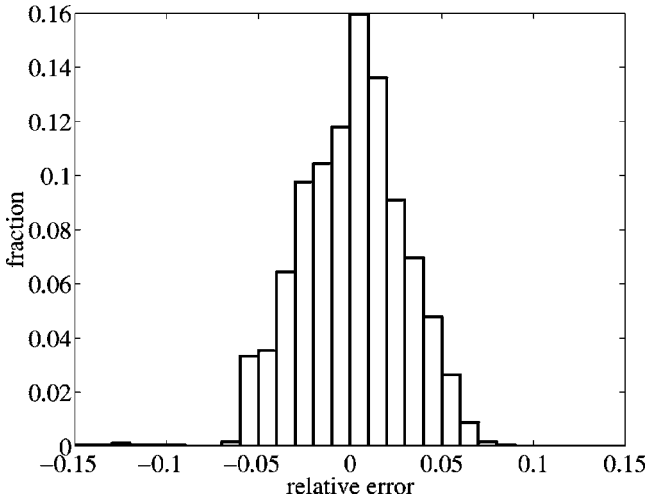

FIG. 12. The relative error (i.e., difference between MC simulation and experiment relative to the maximum dose) tallied in the region where the dose lies in between the lower threshold 10% and the upper threshold 100% of the maximum dose. This histogram shows the fraction of the simulated data points with a certain relative error for $E=21.6$ MeV and $B=3.03$ T.

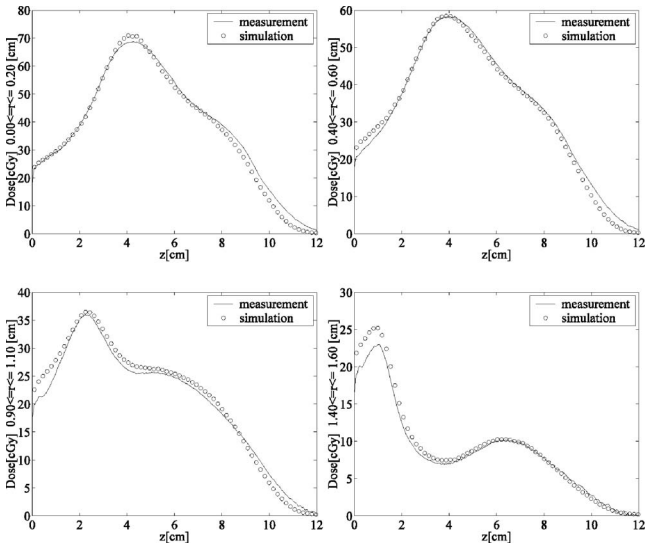

FIG. 13. The measured and simulated electron depth dose curves along the central axis, 0.5, 1.0, and 1.5 cm away from the central axis for $E=21.6$ MeV and $B=3.03$ T.

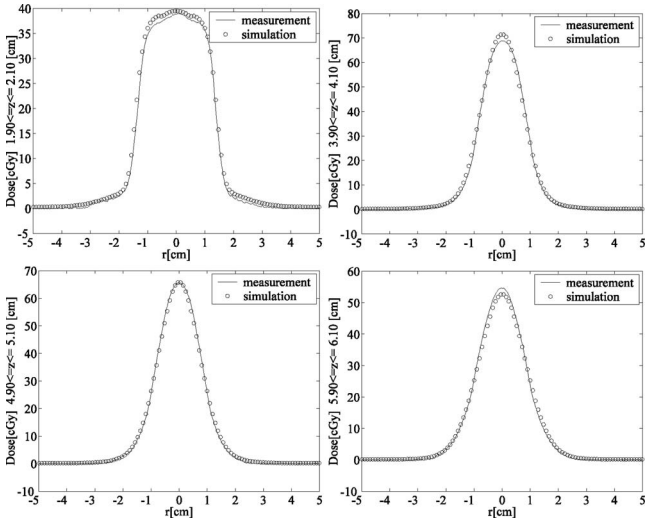

FIG. 14. The measured and simulated electron radial dose profiles at depth 2, 4, 5, and 6 cm for $E=21.6$ MeV and $B=3.03$ T.

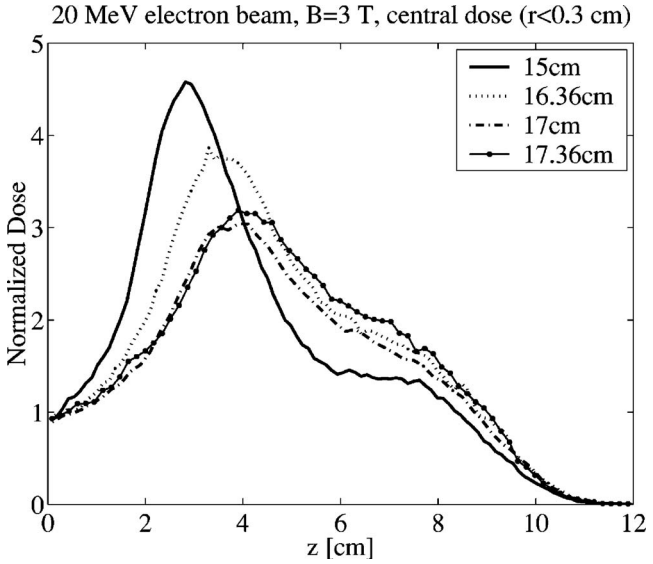

FIG. 16. This graph shows the depth dose profiles when the phantom was placed at different longitudinal positions in the magnetic field, where electron energy is 20 MeV and $B=3$ T. A sharp peak in the dose profile can be formed at the optimal position.

out the magnetic field, additional measurements of the surface dose should be made in order to find the cause of the discrepancies.

Different dose profiles can be formed if the axial position of the phantom (or of course the patient) can be changed while the beam energy and the strength of the magnetic field are fixed. Our MC simulations show that the longitudinal "squeezing" effect can be greater if the front surface of the phantom is about 15 cm away from the field center (Fig. 16). The enhanced dose peak becomes sharper at this position which implies that minimum spread-out of the dose can be achieved with a good combination of beam energy, field strength, and displacement of the phantom/patient (or the field). Likewise, since the solenoid focusing the electron beam acts as a simple lens, displacing the object (incident beam) leads to a known displacement of the image (focused beam). Thus the electron beam can be scanned in the transverse plane as well as intensity modulated for radiation therapy. All of these appear to be clinically viable options in an actual treatment scenario.

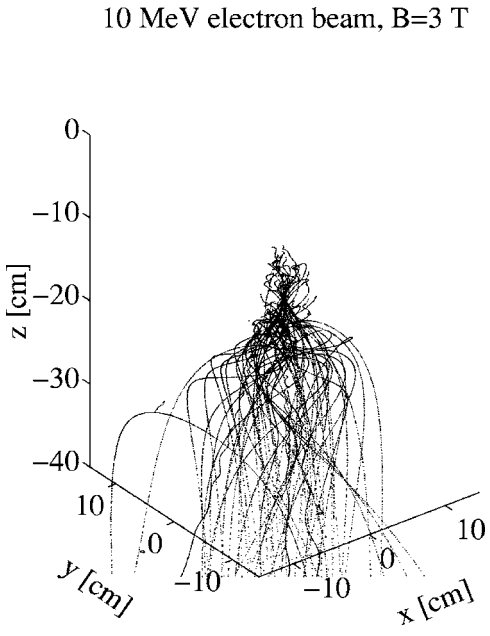

FIG. 15. Three-dimensional plot of the electron tracks near and inside the phantom without the aluminum collimator. The front surface of the phantom is located at $z=-17.16$ cm. The magnetic field center is at the origin ($B=3$ T). The electron beam ($E=10$ MeV) goes in the positive z direction. Here we use 10 MeV instead of 20 MeV electrons to show the "mirror" effect prominently.

B. Photon beams

In addition to the data for electron beam-dose profiles, the experiment[14] also obtained limited data on magnetic confinement of the dose profile for photon beams. In this case the secondary electrons produced by the photons are confined by the magnetic field and hence so is the resulting dose. This potentially could be useful in photon beam therapy as often these secondary electrons can propagate through low-density regions creating extraneous dose to healthy tissue.[9,10] However, the experimental setup was not optimized to demonstrate the reduction of penumbra with magnetic confinement.[14] First, the thickness of the aluminum collimator was not enough to block the photon beam. Second, a large amount of scattered electrons produced in the surrounding air was trapped by the magnetic field and formed a high surface dose. Therefore, our simulation here is used only to reproduce and understand the experiment.

Since the exact geometry of the parts in the gantry head that generates photons was not known, the simulation starts from a photon source with a specific energy distribution, which is not verified with experiments. Nonetheless, the present MC simulations again appear to reproduce qualitatively the existing experimental data[14] (Fig. 17). However, as

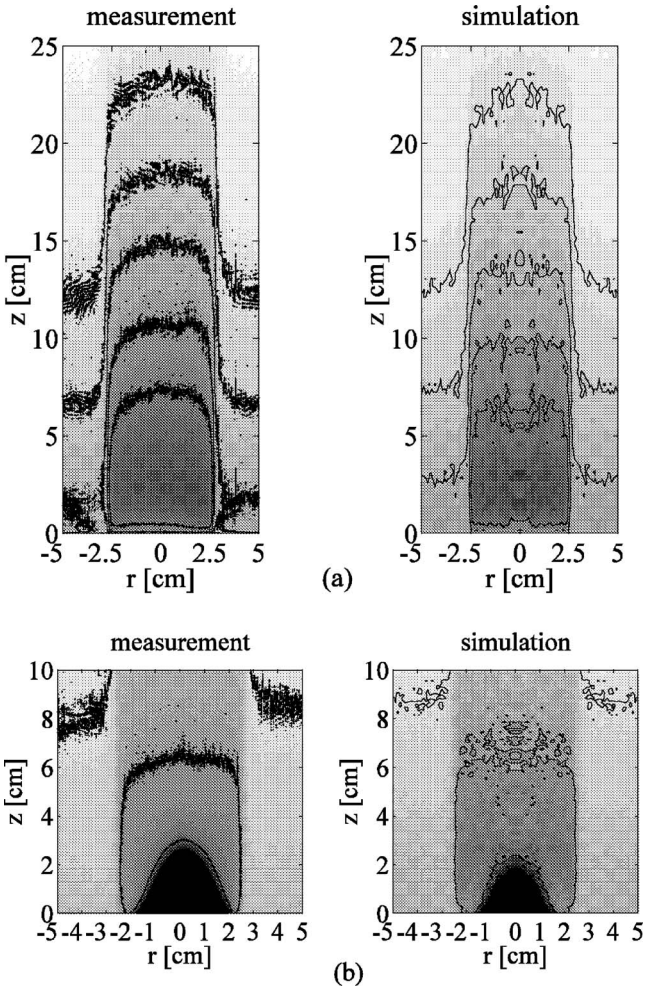

FIG. 17. 10 MV photon beam dose distributions. (a) Comparison of the experimental result (left) with the simulation (right) for $B=0$ T. The 50%, 60%, 70%, 80%, and 90% isodose lines are shown. The dose is scaled to 100% at 3 cm on the central axis. (b) Comparison of the experimental result (left) with the simulation (right) for $B=3.03$ T. The 50%, 80%, and 100% isodose lines are shown. The dose is scaled to 100% at 3 cm on the central axis.

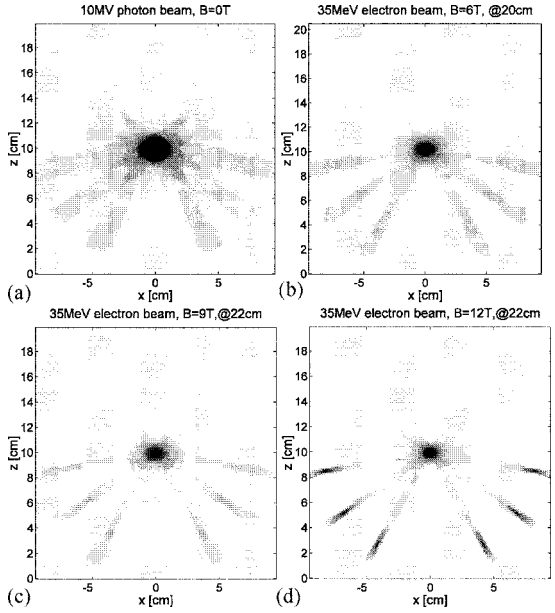

FIG. 18. (a) upper left: dose profile for 10 MV photon beams. (b) Upper right: dose profile for 35 MeV electron beam in 6 T solenoid magnetic field. (c) Lower left: dose profile for 35 MeV electron beam in 9 T solenoid magnetic field. (d) Lower right: dose profile for 35 MeV electron beam in 12 T solenoid magnetic field. We can see the effect of increasing the strength of the magnetic field from (b) to (d). [(a)–(d) all have the same aperture of the aluminum collimator.]

noted, the data were taken with the uniform-density phantom. It thus does not clearly demonstrate that the longitudinal magnetic field can enhance the dose in low-density regions. Additional data using a nonuniform (e.g., a tissue-lung) phantom are needed to provide a more stringent test of the MC simulations.

It was noted that in the experiment the surface dose for the photon beam was intensified when the magnetic field was applied.[14] The present calculations show that this was due to the magnetic field trapping and focusing scattered secondary electrons that were produced in the air by the incident photon beam. Our simulation shows that the surface dose decreases if the volume of surrounding air is reduced.

IV. DISCUSSION

A. Simulation of multibeam electron dose profiles

Since relatively compact electron accelerators, with energy of 20–100 MeV, together with large-bore, high-field superconducting solenoid magnets are either commercially available now or feasible in the near future,[15] we have done simulations in order to further demonstrate the possibilities of magnetically confined electron-beam radiation therapy. As an example, we have done a simple simulation of a multibeam stereotactic treatment dose profile with 35 MeV electron beams, which would be typical of a modest-size microtron adapted for clinical use. 20 MeV electron beams are not energetic enough to treat a position as deep as 10 cm. A skull plus tissue phantom was modeled as 0.6-cm-thick bone followed by uniform tissue in a 20-cm-diam phantom set edge-wise to a magnetically confined electron beam. Six electron beams each with energy of 35 MeV were used with a longitudinal solenoid magnetic field of 6 T. The latter was suitably arranged together with aluminum collimator of 2 cm aperture to provide optimal dose at the center of the skull-tissue phantom (Fig. 18). As can be seen in the simulations, it appears possible to provide a very high dose in a relatively small volume while avoiding critical regions (Figs. 19 and 20). The dose peak was the superposition of the six individual confined doses. Without the magnetic field, the dose would spread out in the region. As seen from a comparison between Figs. 18(a) and 18(b), the dose after the hot spot was greatly reduced in the case of electron beams. Even stronger fields lead to better dose confinement [Figs. 18(b)–18(d)]. As indicated by Fig. 16, the position of the phantom in the magnetic field can significantly affect the dose profile. The dose near the entrance in Fig. 18(d) was increased due to the increase of the magnetic field strength. The position of the phantom in the magnetic field could be

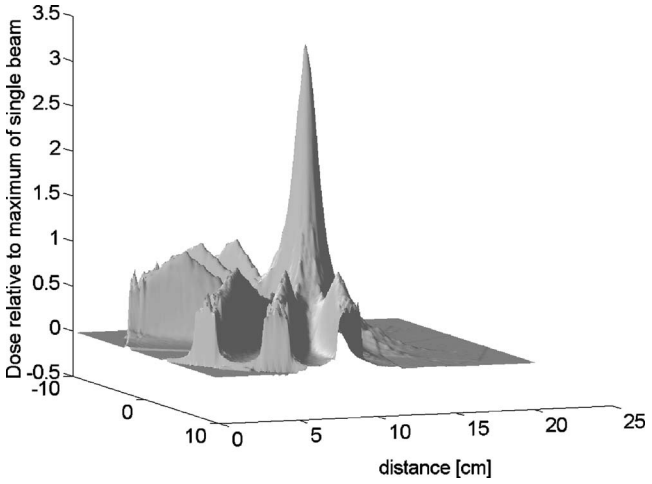

FIG. 19. Two-dimensional dose plot of the multibeam 35 MeV electron dose profile with a 6 T solenoid magnet.

tuned to reduce the dose near the entrance. All these factors should be taken into consideration in a real treatment planning system.

Again, of course, experimental data would provide a more stringent test of this but these simulations suggest that magnetically confined electron beams using high-field solenoids effectively could be used in multibeam stereotactic treatments. A common on-site electron accelerator facility could be used to provide both magnetically confined photon and electron beam radiation therapy treatment. The issue of providing a suitable magnetic-field configuration in a clinical setting has previously been discussed.[15] Very large bore, high-field superconducting solenoids including split-coil magnets are commercially available with some systems requiring no cryogens (LN or LHe). The latter are particularly well suited for mounting on a gantry suitable for stereotatic treatment. The patient could be placed between the Helmholtz coil pair during the treatment much like those in open bore MRI scanners. Also, it recently has been shown that an array of permanent magnets can be utilized to provide magnetic collimation for electrons.[27] As noted earlier, unlike a transverse magnetic field, a longitudinal magnetic field does not deflect the incident primary electron beam, hence the magnet can be an integral part of the electron accelerator gantry.

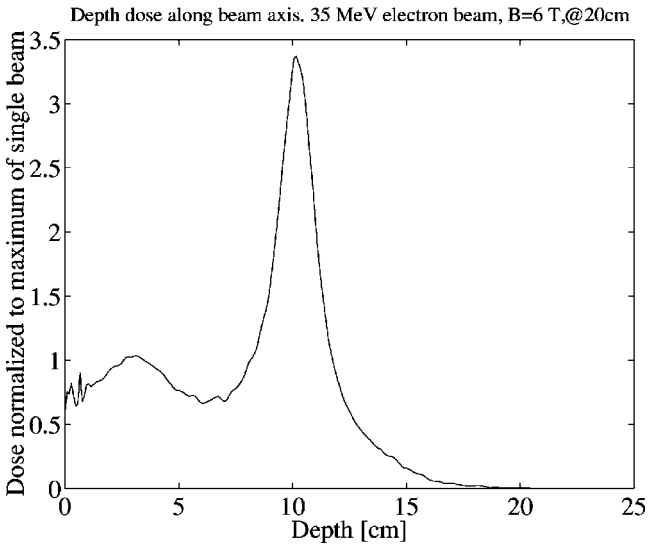

FIG. 20. The dose along a beam axis with electron energy of 35 MeV and peak value of the solenoid magnetic field 6 T.

B. Possible dependence of relative biological effectiveness on magnetic fields

As previously noted by others,[3,6,8] since the trajectories of the low-energy secondary electrons primarily responsible for radiation damage and hence the relative biological effectiveness (RBE) are altered in the presence of high magnetic fields, it is possible that RBE may depend on the magnetic field. If this is the case, RBE as a function of the field strength B would need to be determined and modeled for any magnetically confined radiation therapy beam. While a few measurements of this type have been done,[28,29] more complete measurements are needed.

V. CONCLUSION

The experimental dose profiles are generally reproduced in the simulation to within a few percent. By comparing the simulations with the experiments, we demonstrate that the nonuniform longitudinal magnetic field generated by a solenoid can provide both transverse and longitudinal confinement of an electron beam dose profile. The three-dimensional confinement results from focusing effect of the magnetic lens, reduction of lateral scattering of the electrons, and the mirror effect of the magnetic field. Our results show that the MC code PENELOPE has the basic capability of calculating the dose with realistic magnetic fields. However, the primary electron beam energy and the beam-line geometry need to be carefully verified and modeled in order to get an accurate simulation.

From our simulations, we can see that electron dose profiles can be manipulated by the appropriate combination of the beam energy, the strength of the magnetic field, and the position of the target media in the magnetic field. Stereotactic treatment appears possible using magnetically confined electron beams. The physical collimation and the magnetic confinement have to be suitably adjusted to optimize the dose profile. Since intense primary electron beams are readily available, a high dose rate can be obtained.

ACKNOWLEDGMENTS

We would like to thank Indrin Chetty for providing us the geometry of some of the components inside the gantry head. This work was supported by a Munn Foundation Grant from the University of Michigan Comprehensive Cancer Center and NSF Grants Nos. PHY-02-44989 and 03-54828.

[a]Electronic mail: yuchen@umich.edu

[1]W. H. Bostick, "Possible techniques in direct-electron-beam tumor therapy," Phys. Rev. **77**, 564–565 (1950).

[2]C. C. Shih, "High energy electron radiotherapy in a magnetic field," Med. Phys. **2**, 9–13 (1975).
[3]D. P. Whitmire, D. L. Bernard, M. D. Peterson, and J. A. Purdy, "Magnetic enhancement of electron dose distribution in a phantom," Med. Phys. **4**, 127–131 (1977).
[4]D. P. Whitmire, D. L. Bernard, and M. D. Peterson, "Magnetic modification of the electron-dose distribution in tissue and lung phantoms," Med. Phys. **5**, 409–417 (1978).
[5]R. Nath and R. J. Schulz, "Modification of electron-beam dose distribution by transverse magnetic fields," Med. Phys. **5**, 226–230 (1978).
[6]B. R. Paliwal, A. L. Wiley, Jr., B. W. Wessels, and M. C. Choi, "Magnetic field modification of electron-beam dose distributions in inhomogeneous media," Med. Phys. **5**, 404–408 (1978).
[7]M. S. Weinhous, R. Nath, and R. J. Schulz, "Enhancement of electron beam dose distributions by longitudinal magnetic fields: Monte Carlo simulations and magnet system optimization," Med. Phys. **12**, 598–603 (1985).
[8]A. F. Bielajew, "The effect of Strong Longitudinal magnetic fields on dose deposition from electron and photon beams," Med. Phys. **20**, 1171–1179 (1993).
[9]S. J. Wadi-Ramahi, S. A. Naqvi, and J. C. H. Chu, "Evaluating the effectiveness of a longitudinal magnetic field in reducing underdosing of the regions around upper respiratory cavities," Med. Phys. **28**, 1711–1717 (2001).
[10]S. A. Naqvi, X. A. Li, S. W. Ramahi, J. C. Chu, and S. Ye, "Reducing loss in lateral charged-particle equilibrium due to air cavities present in x-ray irradiated media by using longitudinal magnetic fields," Med. Phys. **28**, 603–611 (2001).
[11]L. Reiffel, A. Li, J. Chu, R. W. Wheatley, S. Naqvi, R. Pillsbury, and A. Saxena, "Control of photon beam dose profiles by localized transverse magnetic fields," Phys. Med. Biol. **45**, N177–N182 (2000).
[12]X. A. Li, L. Reiffel, J. Chu, and S. Naqvi, "Conformal photon-beam therapy with transverse magnetic fields: Monte Carlo study," Med. Phys. **27**, 1447 (2000).
[13]D. Jette, "Magnetic fields with photon beams: Monte Carlo calculations for a model magnetic field," Med. Phys. **27**, 2726–2738 (2000).
[14]D. W. Litzenberg, B. A. Fraass, D. L. McShan, T. W. O'Donnell, D. A. Roberts, F. D. Becchetti, A. F. Bielajew, and J. M. Moran, "An apparatus for applying strong longitudinal magnetic fields to clinical photon and electron beams," Phys. Med. Biol. **46**, pp. N105–N115 (2001).
[15]F. D. Becchetti, D. W. Litzenberg, J. M. Moran, T. W. O'Donnell, D. A. Roberts, B. A. Fraass, D. L. McShan, and A. F. Bielajew, "Magnetic confinement of radiotherapy beam-dose profiles," *Proceedings of Cyclotrons and Their Applications 2001, Sixteenth International Conference* (AIP Press, New York, 2001), pp. 44–46.
[16]F. D. Becchetti, J. M. Sisterson, and W. R. Hendee, "Point/Counterpoint: High energy electron beams shaped with applied magnetic fields could provide a competitive and cost-effective alternative to proton and heavy-ion radiotherapy," Med. Phys. **29**, 2435–2437 (2002).
[17]J. Baró, J. M. Fernández-Varea, and F. Salvat, "PENELOPE: An algorithm for Monte Carlo simulation of the penetration and energy loss of electrons and positrons in matter," Nucl. Instrum. Methods Phys. Res. B **100**, 31–46 (1995).
[18]J. Sempau, E. Acosta, J. Baró, J. M. Fernández-Varea, and F. Salvat, "An algorithm for Monte Carlo simulation of coupled electron-photon transport," Nucl. Instrum. Methods Phys. Res. B **132**, 377–390 (1997).
[19]J. Sempau, A. Sánchez-Reyes, F. Salvat, H. Oulad ben Tahar, S. B. Jiang, and, J. M. Fernández-Varea, "Monte Carlo simulation of electron beams from an accelerator head using PENELOPE," Phys. Med. Biol. **46**, 1163–1186 (2001).
[20]R. D. Stewart, W. E. Wilson, J. C. McDonald, and D. J. Strom, "Microdosimetry properties of ionizing electrons in water: A test of the PENELOPE code system," Phys. Med. Biol. **47**, 79–88 (2002).
[21]R. L. Stern, "Design and utilization of an air-core superconducting-solenoid nuclear-reaction-product spectrometer," Ph.D. dissertation of the Department of Physics, the University of Michigan, 1987, pp. 26–31.
[22]W. Liu, "Production and use of radioactive ion beams for measurements of nuclear reactions," Ph.D. dissertation of the Department of Physics, the University of Michigan, 1990, pp. 17.
[23]E. Nardi, G. Barnea, and C. Ma, "Electron beam therapy with coil-generated magnetic fields," Med. Phys. **31**, 1494–1503 (2004).
[24]I. J. Chetty, J. M. Moran, T. S. Nurushev, D. L. McShan, B. A. Fraass, S. J. Wilderman, and A. F. Bielajew, "Experimental validation of the DPM Monte Carlo code using minimally scattered electron beams in heterogeneous media," Phys. Med. Biol. **47**, 1837–1851 (2002).
[25]D. Sheikh-Bagheri and D. W. O. Rogers, "Sensitivity of megavoltage photon beam Monte Carlo simulations to electron beam and other parameters," Med. Phys. **29**, 379–390 (2002).
[26]J. D. Jackson, "Classical Electrodynamics," 3rd ed., ISBN 0-471-30932-X, pp. 594–596.
[27]L. Ma, "Dosimetric properties of magnetically collimated electron beams for radiation therapy," Med. Phys. **31**, 2973–2977 (2004).
[28]R. Nath, R. J. Schulz, and P. Bongiorni, "Response of mammalian cells irradiated with 30MV X-rays in the presence of a uniform 20-kilogauss magnetic field," Int. J. Radiat. Biol. **38**, 285–292 (1980).
[29]S. Rockwell, "Influence of a 1400-gauss magnetic field on the radiosensitivity and recovery of EMT6 cells *in vitro*," Int. J. Radiat. Biol. **31**, 153–160 (1977).